ELSEVIER

Polymer 42 (2001) 6161–6172

polymer

www.elsevier.nl/locate/polymer

# Effect of glass fiber and maleated ethylene–propylene rubber content on the impact fracture parameters of nylon 6

D.M. Laura, H. Keskkula, J.W. Barlow, D.R. Paul*

*Department of Chemical Engineering and Texas Materials Institute, University of Texas at Austin, CPE 3.454, Austin, TX 78712, USA*

Received 17 October 2000; received in revised form 18 December 2000; accepted 20 December 2000

**Abstract**

The impact fracture parameters of blends of nylon 6 and maleated ethylene–propylene rubber (EPR-*g*-MA) reinforced with glass fibers as a function of glass fiber and EPR-*g*-MA content were examined. Both the linear elastic fracture mechanics (LEFM) model and a modified essential work of fracture (EWF) model were used to analyze the data. It was found that the addition of EPR-*g*-MA to unreinforced nylon 6 increased the EWF parameters $u_o$ and $u_d$ defined by $U/A = u_o + u_d\ell$, where $U/A$ is the total fracture energy per unit area and $l$ is the ligament length. Beyond a critical rubber content, which coincided with the ductile-to-brittle transition, there was a large increase in $u_d$. When glass fiber reinforcement was used without rubber toughening, the EWF model was unable to model the observed fracture response. On the other hand, the LEFM model adequately described the fracture behavior, and it was found that the critical strain energy release rate, $G_{IC}$, increased with increasing glass fiber content. When both glass fiber reinforcement and rubber toughening were used, the $u_o$ increased with increasing EPR-*g*-MA or glass fiber content; whereas, $u_d$ increased with increasing ERR-*g*-MA content or decreasing glass fiber content. 

*Keywords*: Rubber toughened nylon 6; Fiber reinforced; Impact fracture parameters

## 1. Introduction

The incorporation of rubber particles into a thermoplastic polymer matrix is known to improve the impact properties and low temperature toughness of the polymer [1,2]. Under the proper conditions, synergistic effects arise leading to 'super-tough' blends. The energy to fracture such blends may be orders of magnitude higher than the untoughened material. Unfortunately, adding low modulus rubber particles to engineering thermoplastics lowers stiffness and strength. The use of high modulus fibers, on the other hand, can increase the stiffness and strength of an engineering thermoplastic [3]. If discontinuous fibers are used, then the materials can still be injection molded into parts using the same procedure for unreinforced thermoplastic polymers [4]. If the matrix material used is brittle, then glass fiber reinforcement may actually increase fracture energy [5,6]; however, the fracture energy of ductile, highly toughened polymer blends is reduced by the incorporation of glass fibers [5,7–12].

The combination of glass fiber reinforcement and rubber toughening in engineering thermoplastics is a relatively unexplored area. A previous paper investigated the trade-off between tensile properties and Izod impact strength of glass fiber reinforced blends of nylon 6 and maleated ethylene–propylene rubber (EPR-*g*-MA) [12]. The notched Izod impact test is a convenient and simple method of evaluating materials; however, it does not provide a complete picture of the fracture behavior or any information about the mechanisms of deformation. The purpose of this paper is to examine in more detail the fracture behavior of glass fiber reinforced nylon 6/EPR-*g*-MA blends via instrumented impact tests using single-edge notched three-point bend (SEN3PB) specimens.

## 2. Background

Linear elastic fracture mechanics (LEFM) methodologies have been used to measure the critical strain energy release rate ($G_{IC}$) or the critical stress intensity factor ($K_{IC}$) of polymeric materials [13]. According to this model, the total energy to fracture a sample, $U$, is given by the following well-known equation

$$U = G_{IC}tW\phi + U_k, \tag{1}$$

where $G_{IC}$ is the critical strain energy release rate which is a

* Corresponding author. Tel.: +1-512-471-5392; fax: +1-512-471-0542.
*E-mail address:* drp@che.utexas.edu (D.R. Paul).

0032-3861/01/$ - see front matter 
PII: S0032-3861(01)00068-4

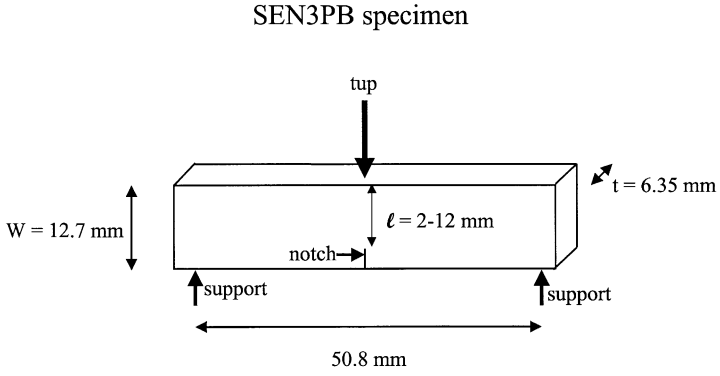


Fig. 1. Single edge notched three point bend specimen displaying width ($W$), thickness ($t$), and ligament length ($\ell$).

material parameter that when properly determined does not depend on specimen geometry. As shown in Fig. 1, $W$ and $t$ are the specimen width and thickness, respectively. The term $U_k$ is the kinetic energy of the test specimen after fracture, and is part of the energy measured by most techniques. The factor $\phi$ is defined by

$$\phi = \frac{C}{dC/d(a/W)}, \tag{2}$$

where $C$ is the specimen compliance and $a$ is the crack length. Expressions for $\phi$ can be determined analytically, experimentally, or can be calculated by standardized formulas and tables [13].

The LEFM method is effective for characterizing brittle polymers; however, ductile polymers, such as rubber-toughened polymer blends, generally do not obey the assumptions of linear elasticity, and the sample thickness required to meet the plain strain requirements is greater than what can be conveniently molded. The $J$-integral method does not rely on any assumption of linear elasticity and is regarded as more appropriate for ductile polymers. This method is restricted to quasi-static loading, and requires specialized equipment for accurate crack growth measurement; however, the requirement on specimen thickness may still be greater than what can be conveniently fabricated.

Mai and coworkers have developed a method to characterize the fracture of ductile materials [14–16] based of Broberg's unified fracture theory [17,18]. According to the model, the total energy required to fracture a sample, $W_f$, can be divided into the essential work of fracture (EWF) in the inner process zone and the non-EWF in the outer, plastic zone. The expression for the total fracture work is

$$W_f = w_e \ell t + \beta w_p \ell^2 t, \tag{3}$$

where $w_e$ is the specific EWF, $w_p$ the non-EWF and has units of energy per unit volume, and $\beta$ is a shape factor. As defined in Fig. 1, $l$ and $t$ are the ligament length and specimen thickness, respectively. For Eq. (1) to apply, the size of the outer plastic zone must scale as $\ell^2$. If the above expression is divided by fracture ligament area ($\ell t$), the following expression for the specific fracture work, $w_f$, is obtained

$$w_f = w_e + \beta w_p \ell. \tag{4}$$

Thus, the specific fracture work should increase linearly with $\ell$, with a slope of $\beta w_p$ and an intercept of $w_e$.

Mai et al. state that this method of analysis requires that the specimen be fully yielded prior to crack initiation, which can easily be assessed for slow testing of double-edge notched tensile specimens typically used by Mai et al. In the current work, we use an instrumented impact test where a single-edge notched specimen is loaded in bending. Complete force-displacement data are obtained which can be integrated to give the fracture energy. Because the testing speed and geometry are quite different from the conditions used by Mai et al., the slope and intercept from plots of $w_f$ versus ligament length may not necessarily have the same physical meanings that have been assigned to $\beta w_p$ and $w_e$. Thus, we use a different nomenclature for these plots, i.e.

$$\frac{U}{A} = u_o + u_d \ell, \tag{5}$$

where $U/A$ is the total fracture energy per unit area, $u_o$ is the limiting specific fracture energy, and $u_d$ is the dissipative energy density. These parameters should be considered phenomenological in nature and are not treated here as material parameters. Rather, the current work is intended to give a greater understanding of the fracture mechanisms of these materials and provide fracture toughness information that is more in depth than simple Izod or Charpy testing.

In cases where the fracture process is described by the LEFM model represented in Eq. (1), the data may still be presented in the format of Eq. (5), i.e. a plot of $U/A$ versus $\ell$. Rearrangement of Eq. (1) gives

$$\frac{U}{A} = G_{IC} W\left(\frac{\phi}{\ell}\right) + \frac{U_k}{\ell t}. \tag{6}$$

The first term on the right-hand side of Eq. (6) increases when ligament length becomes very long, while the second term always decreases with increasing ligament length. The net result of these two terms is a function that initially

Table 1
Materials used in this study

| Material designation | Source | Manufacturer's designation | Description |
|---|---|---|---|
| Nylon 6 | Allied signal | Capron B73WP | Nylon 6, $\bar{M}_n = 22,000$ End-group content: $NH_2 = 47.9$ μ eq/g COOH = 43.0 μ eq/g |
| EPR-*g*-MA | Exxon chemical | Exxelor 1803 | Ethylene–propylene rubber 43 wt% ethylene 53 wt% propylene 1.14 wt% grafted maleic anhydride |
| BKV 30 | Bayer | Durethan BKV 30 | Glass fiber reinforced nylon 6 30 wt% well-bonded, discontinuous glass fibers |

decreases (has a negative slope) as a function of ligament length then increases as a function of ligament length for longer ligaments. This is in contrast to the EWF analysis above; however, it should be noted that the LEFM equations only strictly apply to brittle samples were $U$ is the energy to peak load. The EWF model employs the total energy to fracture the sample and is said to apply for both ductile and brittle materials.

## 3. Experimental

Table 1 describes the materials used in this study. Capron B73WP is a commercial nylon 6 material having $\overline{M_n} = 22,000$. The glass fiber reinforced material is Durethan BKV 30 and contains 30 wt% discontinuous glass fibers, diameter = 13 μm.The average length of these glass fibers in the final molded part is 300 μm, yielding an average aspect ratio ($l/d$) of 23. The ethylene-propylene rubber (EPR-*g*-MA) contains 1.14 wt% grafted maleic anhydride for reaction with the amine end groups of nylon 6. This EPR-*g*-MA has been used to produce super-tough nylon 6 blends [19–22].

In order to produce molded materials containing both glass fibers and EPR-*g*-MA, a 'mother blend', containing only nylon 6 and EPR-*g*-MA, was compounded in an extruder. Pellets of this mother blend were dry mixed with BKV 30 pellets prior to injection molding. The fact that the glass fibers were compounded into the BKV 30 pellets by the supplier using effective coupling chemistry means that the fiber–matrix bond remains the same regardless of the amount of subsequent rubber addition; hence, the degree of fiber–matrix adhesion is not a variable in this study. Extrusion compounding of nylon 6 and EPR-*g*-MA was performed in a Killion single-screw extruder ($L/D = 30$, $D = 2.54$ cm), equipped with an intensive mixing head, at 240°C using a screw speed of 40 rpm. A mixture of these pellets and BKV 30 pellets was loaded directly into the hopper of the injection molding machine such that the final part had the proper amount of nylon 6, glass fibers and EPR-*g*-MA. Injection molding was performed in an Arburg Allrounder operating at an injection pressure of 70 bar and holding pressure of 35 bar. Temperatures were set at 240°C in the feed zone, up to 270°C in the nozzle, while the mold was held at 80°C. Screw speed was maintained at 150 rpm. Izod bars, thickness = 6.35 mm and width = 12.7 mm, were molded for impact testing. This method has the limitation that a material containing large amounts of fiber and rubber cannot be made due to material balance and processing constraints. For example, for compositions containing 20 wt% rubber, it is not possible to generate materials by this method that contain more than 20 wt% glass fibers. All materials were dried in a vacuum oven at 80°C for at least 16 h prior to melt processing. Molded bars were stored in vacuum descicators for at least 24 h prior to testing such that all measurements were made in the dry-as-molded (DAM) state.

A Dynatup drop tower model 8200 was used for all instrumented impact testing. Testing was performed at 3.5 m/s with a falling mass of 14 kg. For each composition, 24 specimens like those in Fig. 1 were prepared with ligament lengths ranging between 2 and 10 mm; a sharp notch was formed by inserting a fresh razor blade into each specimen. Load versus time data and tup speed were obtained by computerized data acquisition. Load versus displacement data could then be easily obtained and integrated to measure fracture energies. Brittle materials tested in this manner lead to severe oscillations in the load–displacement curve. This masks the true fracture behavior of the material and makes data analysis difficult. As a result, all materials used in this study were tested with a rubber material over the tup to dampen the oscillations. Since the total energy to fracture the specimen is considered in the analysis given above, as opposed to the energy to peak load for example, the only error that should result from this damping is the hysteresis associated with loading and unloading the rubber pad during the testing. This contribution to the total energy is negligible for the current materials.

## 4. Results and discussion

### 4.1. Effect of rubber toughening

Fig. 2 shows load–displacement diagrams for nylon 6 specimens of nearly the same ligament length containing 0 and 10 wt% EPR-*g*-MA. Under the stress conditions imposed here, nylon 6 is quite brittle. For the neat nylon 6 specimen, the load reaches, approximately, 190 N before sharply dropping off in the manner characteristic of the

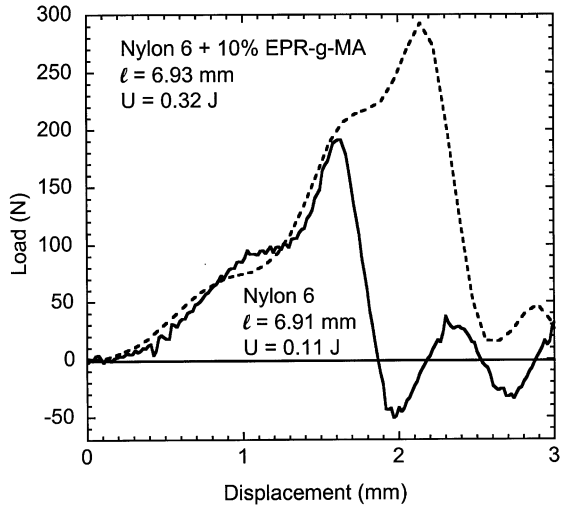


Fig. 2. Load–displacement diagram for SEN3PB specimens of neat nylon 6 and nylon 6/EPR-*g*-MA (90/10). Ligament lengths ($\ell$) and total fracture energies ($U$) are noted in the figure.

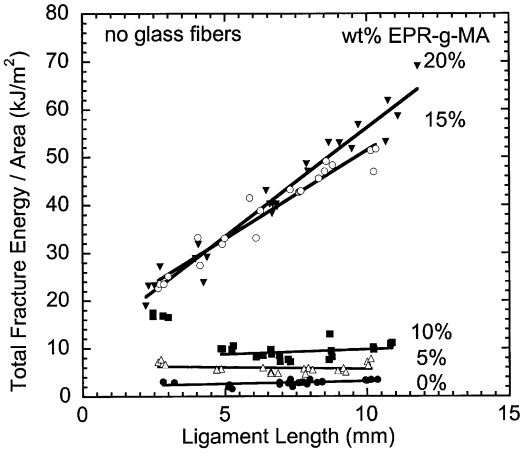


Fig. 4. Total fracture energy per unit area of fracture surface (area $= \mathcal{L}^* t$) versus ligament length for unreinforced nylon 6 containing from 0 to 20 wt% EPR-*g*-MA. The lines drawn represent the best fit of this data to Eq. (5).

fracture of brittle materials. Oscillations in the recorded load are generally observed after a brittle fracture; however, these oscillations do not contribute to the measured fracture energy. The material containing 10 wt% EPR-*g*-MA also exhibits brittle fracture; however, in this case, fracture does not occur until a much higher load and the tup travels further prior to specimen breakage due to the additional ductility provided by the rubber phase. The rubber-toughened specimen is both more ductile and stronger under these testing conditions, and the fracture energy is 0.32 versus 0.11 J for the unmodified nylon 6 specimen.

When 15 wt% or more of EPR-*g*-MA is added to the nylon 6 material there is a large increase in fracture energy. Fig. 3 compares the load–displacement plots for a specimen

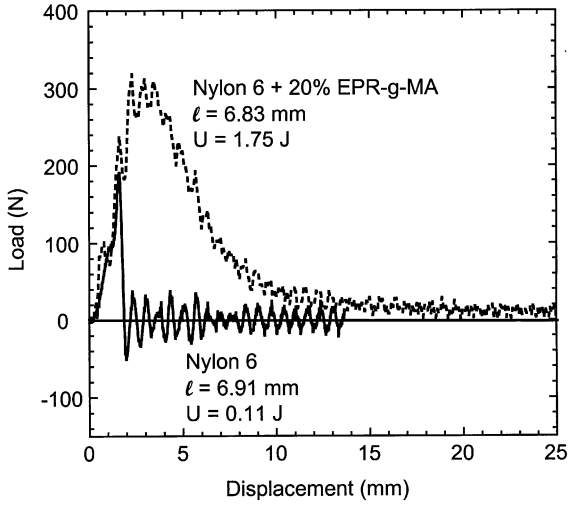


Fig. 3. Load–displacement diagram for SEN3PB specimens of neat nylon 6 and nylon 6/EPR-*g*-MA (90/10). Ligament lengths ($\ell$) and total fracture energies ($U$) are noted in the figure.

containing 20 wt% EPR-*g*-MA with that of the nylon 6 specimen from Fig. 2. This material shows an increased ultimate load and tup displacement relative to both nylon 6 and the material containing 10 wt% EPR-*g*-MA. The material containing 20 wt% EPR-*g*-MA differs markedly in its fracture behavior after specimen yielding in that the load trails off gradually rather than dropping sharply as seen in Fig. 2. This extended tail after specimen yielding is typical of ductile materials. As a result of the higher stresses and increased ductility, there is a very large increase in fracture energy relative to the materials containing less than 15 wt% EPR-*g*-MA. The total fracture energy of the material containing 20 wt% EPR-*g*-MA in Fig. 3 is 1.75 J compared to 0.11 J for a neat nylon 6 specimen of nearly the same ligament length.

Fig. 4 shows plots of specific fracture energy versus ligament length, as suggested earlier, for nylon 6 materials containing various amounts of EPR-*g*-MA. Up to rubber contents of 10 wt% EPR-*g*-MA the slope of these lines, $u_d$, remains essentially zero. According to the theory discussed above, this means that all of the fracture work is done in the region near the fracture surface and very little energy is dissipated in the outer, plastic zone. The addition of up to 10 wt% rubber increases the total fracture energy as noted above; however, there is no significant increase in the slopes for the first three materials shown in Fig. 4, but the intercept, $u_o$, is increased. Furthermore, there is no evidence of any stress whitening away from the fracture surface for the specimens used to generate these lines. This indicates that the increase in total fracture energy upon the addition of 5 or 10 wt% of rubber is the result of processes which occur in the fracture process zone. Samples containing 10 wt% EPR-*g*-MA undergo a ductile–brittle transition with respect to ligament length. Specimens with short ligament lengths are ductile and exhibit high specific fracture energy while those with ligaments longer than 3 mm fail in a brittle

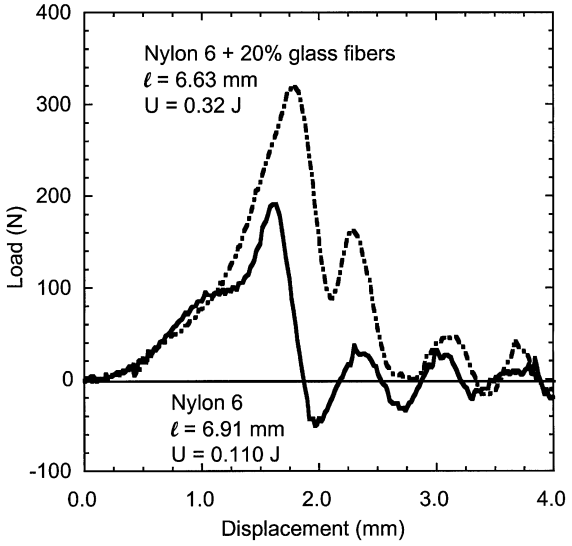


Fig. 5. Load–displacement diagram for SEN3PB specimens of neat nylon 6 and nylon 6/glass fiber (80/20). Ligament lengths ($\ell$) and total fracture energies ($U$) are noted in the figure.

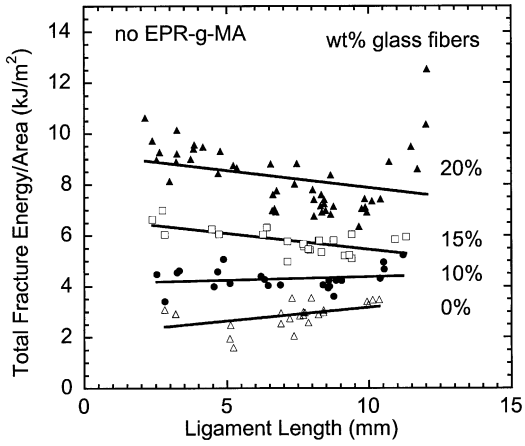


Fig. 6. Total fracture energy per unit area of fracture surface (area = $\ell^* t$) versus ligament length for nylon 6 containing from 0 to 20 wt% glass fibers and no EPR-*g*-MA.

manner. This type of transition in fracture behavior has been seen elsewhere [23–25]. For this case, only the brittle samples were used in the data regression to form the line shown in Fig. 4.

At 15 wt% EPR-*g*-MA, there is a large change in the total fracture energy and in the slope of these plots. A previous paper noted the onset of ductile behavior at the same EPR-*g*-MA content [12]. This increase in fracture energy also coincides with an increase in stress whitening that extends below the fracture surface of these materials. A large stress whitened zone is also present in the shorter ligaments of the material that contains 10 wt% EPR-*g*-MA and is also accompanied by an increase in fracture energy. This stress whitening provides visual evidence of energy absorbing processes that occur away from the fracture surface and corroborates the physical interpretation of the slope of these plots, $u_d$. As the rubber content of these blends increases, the intercept, $u_o$, increases as well. If we can accept the physical interpretation of this intercept, then this indicates that the rubber particles contribute to the fracture energy of a material at the fracture surface as well as in the outer plastic zone.

### 4.2. Effect of glass fibers

Fig. 5 shows load–displacement diagrams for neat nylon 6, from Fig. 2, and a nylon 6 specimen containing 20 wt% glass fibers. Glass fibers are well known to embrittle ductile matrices; however, under these conditions (high-speed, sharp notch) nylon 6 behaves in a brittle manner. As a result, there is no appreciable decrease in the displacement of the tup at specimen failure for the glass fiber containing material relative to the unreinforced nylon 6. The glass fiber containing material does, however, reach a much higher load than the unreinforced nylon 6 as expected for a reinforced material. Because fracture work is the area under a load displacement curve such as Fig. 5, the fact that glass fiber reinforced material reaches higher loads without significant reduction in the amount of deformation results in higher total fracture energy for the reinforced material relative to neat nylon 6.

Traditionally, fiber pullout and fiber–matrix debonding have been cited as the energy absorbing mechanisms that lead to higher fracture energies in fiber reinforced materials [26–31]; fiber pullout energy is generally considered to be the dominant contribution [29–31]. On the other hand, Shiao et al. [32] and Chua et al. [33] give evidence that fiber pullout energy is insufficient to explain the increase in fracture toughness brought about by the incorporation of glass fibers into engineering thermoplastic matrices. Shiao et al. [32] and Gupta et al. [28] attributed increased matrix plasticity, particularly at fiber ends, to be responsible for increased fracture toughness in their slow strain rate tests. Lauke et al. [31] indicated that at slow testing speeds matrix deformation may dominate, but under dynamic (impact) loading conditions the matrix fractures in a brittle manner and fiber pullout dominates when fibers are of a subcritical length, although the implications for longer fibers are not indicated. In the current study, fibers above the critical length were studied [12] at high testing speeds, and it appears that the higher stresses that develop in glass fiber reinforced materials without loss of deformation is the cause for the increase in fracture energy.

Fig. 6 shows plots of $U/A$ versus ligament length for nylon 6 containing from 0 to 20 wt% glass fibers. These plots are of the form suggested by Eq. (4), and the lines drawn are the best fit of this model to the data. Clearly, the EWF model does not provide a very good description of the data; however, some trends can be noted. At a fixed ligament length, the fracture energy increases steadily with glass fiber content suggesting higher values of $u_o$.

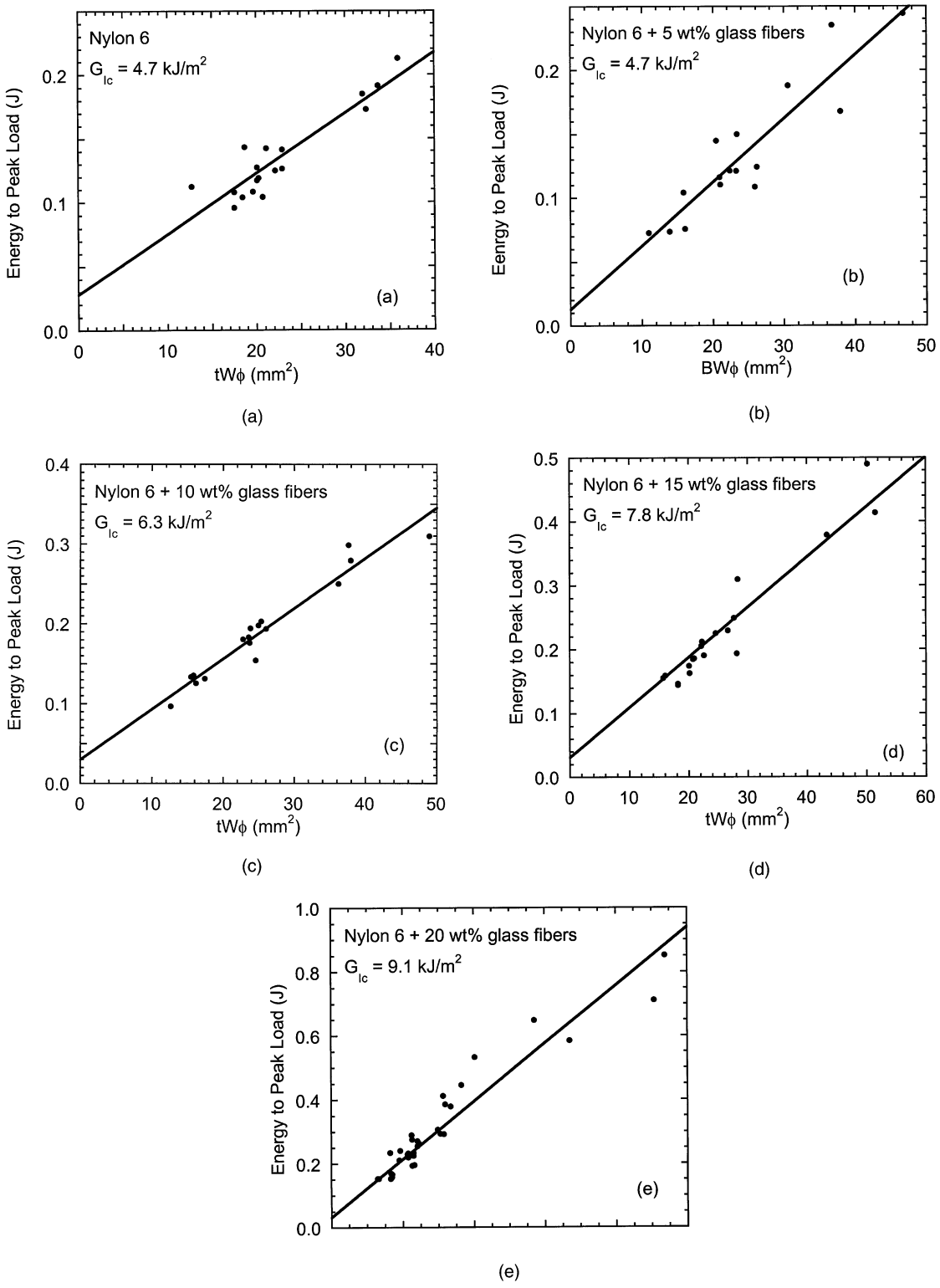


Fig. 7. Energy to peak load versus $tW\phi$ for nylon 6 containing:(a) no glass fibers, (b) 5 wt%, (c) 10 wt%, (d) 15 wt%, and (e) 20 wt% glass fibers. The lines shown represent the best fit of the data to Eq. (1) when the sample kinetic energy ($U_k$) is assigned the value calculated from $1/2mv^2$, where $m$ is sample mass and $v$ is the tup velocity (3.4 m/s).

Table 2
$G_{IC}$ for glass fiber reinforced nylon 6

| Glass fiber content (wt%) | Constrained model[a] | | Unconstrained model[b] | |
|---|---|---|---|---|
| | $G_{IC}$ (kJ/m$^2$) | $U_k$ (J) | $G_{IC}$ (kJ/m$^2$) | $U_k$ (J) |
| 0 | 4.7 | 0.028 | 5.3 | 0.013 |
| 5 | 4.4 | 0.029 | 5.0 | 0.013 |
| 10 | 6.3 | 0.030 | 6.2 | 0.032 |
| 15 | 7.8 | 0.031 | 7.8 | 0.020 |
| 20 | 9.1 | 0.032 | 8.5 | 0.056 |

[a] Kinetic energy in the constrained model is assigned the value calculated from $1/2mv^2$, where $m$ is sample mass and $v$ is the tup velocity (3.4 m/s).
[b] In the unconstrained model, $U_k$ is treated as an adjustable parameter in the data fitting.

The incorporation of glass fibers in a brittle matrix increases fracture energy for the reason discussed above. When brittle fibers are imbedded in a brittle matrix, it cannot be expected that this increase in energy occurs by plastic deformation processes away from the fracture surface. Based on these facts, the expected result of the data analysis of Fig. 6 is an increase in $u_o$ while $u_d$ remains essentially zero. This is essentially the observed result; however, these plots also have the interesting feature that the initial slope of these plots is apparently negative. At longer ligament lengths, the fracture energy per unit area begins to increase.

All of the materials represented in Fig. 6 showed brittle failure and can be subjected to the LEFM analysis represented by Eqs. (1) and (6) if the energy to peak load is considered rather than the total fracture energy as in Fig. 6. For this analysis, the kinetic energy ($U_k$) of the fractured specimen can be used as an adjustable parameter or can be set as the kinetic energy of a specimen traveling at the velocity of the tup, such that there is only one adjustable parameter, the critical strain energy release rate. The result of this analysis for the materials from Fig. 6 is shown in Fig. 7.

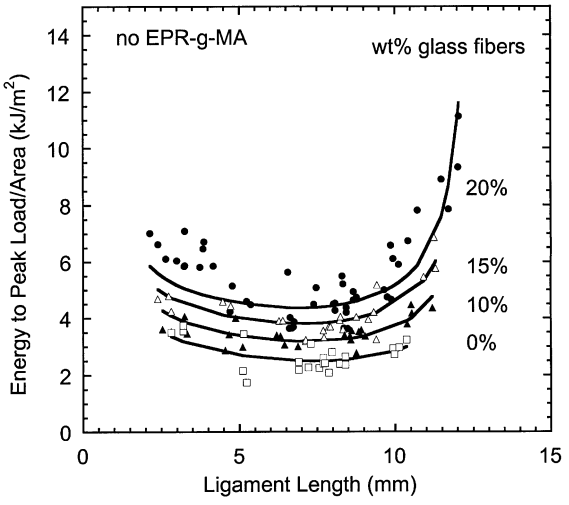


Fig. 8. Energy to peak load per unit fracture surface area (area $= \ell^* t$) versus ligament length. The curves drawn were calculated from Eq. (6) using the data in Table 2.

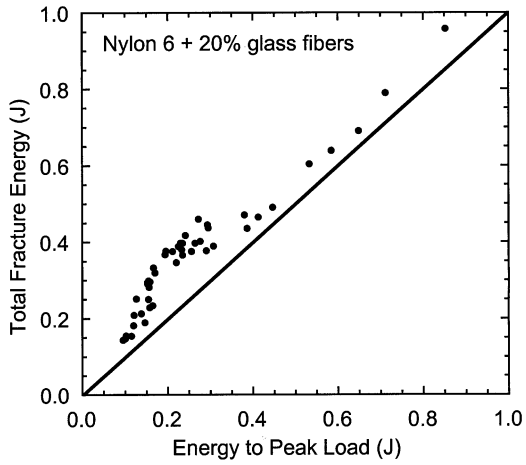


Fig. 9. Total fracture energy versus energy to peak load for nylon 6 containing 20 wt% glass fibers. The line drawn represents the case where the energy to peak load equals the total fracture energy.

In these figures, $U_k$ has been set as if the material were moving at the tup velocity such that there is only one adjustable parameter in Eq. (6). The data fit this model well. Table 2 shows the values of the critical strain energy release for the materials used in this study that contain no rubber for the case, where the kinetic energy has been set before regression and for the case where it is used as an adjustable parameter. The general trend is for the critical strain energy release rate to increase at higher glass fiber contents.

Fig. 8 shows the energy to peak load per unit area versus ligament length for the same specimens in Fig. 6, where the total energy to fracture is plotted. The data in Figs. 6 and 8 show similar trends. The solid lines in Fig. 8 were computed from Eq. (6) by inserting the values for $G_{IC}$ and $U_k$ from Table 2, where the kinetic energy has been calculated from the sample mass and tup velocity rather than treated as an adjustable parameter. The right-hand side of Eq. (6) contains two terms which together capture the trend of these plots. In this model, the kinetic energy is taken to be constant; thus, when normalized by the ligament area, this term is inversely proportional to ligament length, which causes the initial negative slope. The term associated with the parameter $\phi$, on the other hand is initially nearly constant; however, at longer ligament lengths it increases sharply causing the increase in fracture energy per unit area that is seen in these plots. As a result, the LEFM model expressed in Eq. (6) does a much better job of describing the trends of these data than the EWF model expressed in Eqs. (4) or (5). Because the LEFM model and the EWF model are different in that the former is concerned with the energy to peak load only and the latter considers the total fracture energy, it remains to be demonstrated why the data in Fig. 6, where the total fracture energy is shown, should have the same general trend as the data in Fig. 8.

In Fig. 9, total fracture energy is plotted against energy to peak load. The total fracture energy is, of course, somewhat

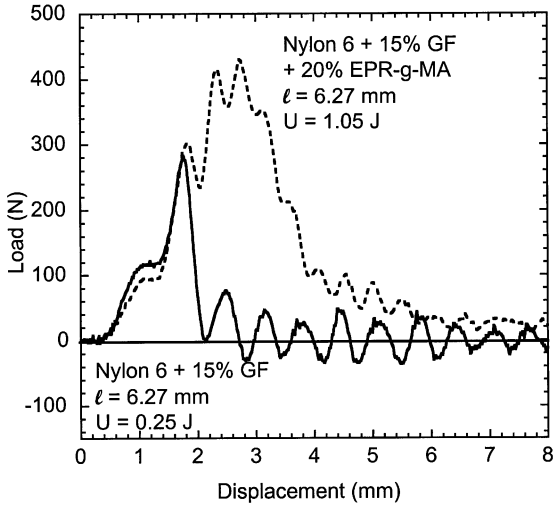


Fig. 10. Load–displacement diagram for SEN3PB specimens of nylon 6/glass fiber (85/15) and (nylon 6/EPR-*g*-MA)/glass fiber [(80/20)/15]. Ligament lengths ($\ell$) and total fracture energies ($U$) are noted in the figure.

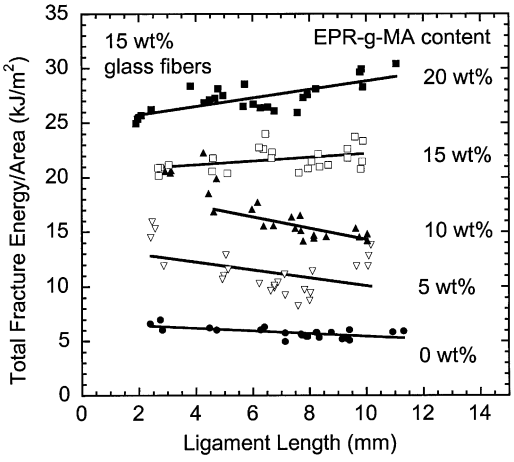


Fig. 11. Total fracture energy per unit area of fracture surface (area $= \mathcal{L}^* t$) versus ligament length for nylon 6 containing from 0 to 20 wt% EPR-*g*-MA and 15 wt% glass fibers. EPR-*g*-MA content is based on the mass of polymer matrix only (nylon 6 + EPR-*g*-MA), and glass fiber content is based on total mass of polymer and glass.

higher than the energy to peak load; however, the data are well correlated. The same correlation exists for the other materials in Fig. 6. It then follows that the general trend of the data in Fig. 6 will be the same as in Fig. 8; therefore, the LEFM model explains why these data initially have a negative slope followed by an increase in fracture energy at longer ligaments. It should also be noted that the two models used to analyze these data do not produce the same general trends and, therefore, are mutually exclusive. The LEFM theory, however, is not applicable to ductile materials which are also considered in this study.

### *4.3. Effect of adding rubber to glass fiber reinforced materials*

Fig. 10 shows load–displacement diagrams for two materials (with and without rubber) reinforced with 15 wt% glass fibers. There are two significant differences in the fracture behavior of these two materials. The specimen containing 20 wt% EPR-*g*-MA reaches a substantially higher peak load, and the decrease in load after the peak is gradual compared to the sharp drop for the material containing no rubber. Furthermore, a greater tup displacement is reached prior to specimen failure in the rubber toughened specimen. Thus, the addition of rubber to the glass fiber reinforced material increases the extent of specimen deformation and the ultimate load during the impact test. This is the same qualitative effect that rubber has on unreinforced nylon 6. As a result, the glass fiber reinforced, rubber-toughened materials have much higher fracture energies than materials containing only glass fibers. For the specimens in Fig. 10, the specimen containing no rubber had a fracture energy of 0.25 J while the material containing 20 wt% EPR-*g*-MA had a fracture energy of 1.05 J.

The data represented as total fracture energy per unit area versus ligament length for materials containing 15 wt% glass fibers and from 0 to 20 wt% EPR-*g*-MA are shown in Fig. 11. The curves shown represent the best fit of this data (neglecting some data at short ligament lengths for reasons mentioned later) to the linear model of Eq. (5). These data indicate that the fracture energy of these materials is increased by the addition of EPR-*g*-MA. The slopes of these plots are negative for materials containing 10 wt% or less EPR-*g*-MA and positive for materials containing 15 wt% or more rubber. This transition from negative to positive values for $u_d$ can be understood by examining the fracture surfaces. For the materials containing 15–20 wt% EPR-*g*-MA, there is stress whitening over the entire ligament length for every fractured specimen. For specimens with short ligament lengths containing 10 wt% EPR-*g*-MA, there is also evidence of stress whitening everywhere on the fracture surface. Ligaments of intermediate length, however, show stress whitening over some portion of their fracture surface, while the samples with the longest ligaments show very little evidence of stress whitening. The materials containing 0 and 5 wt% EPR-*g*-MA show almost no stress whitening at all. These two materials behave in the same manner and have negative slopes for the same reason as those in Fig. 6; however, the material containing 10 wt% EPR-*g*-MA has a slope which is even more negative than these two materials or those seen in Fig. 6. If these observations of stress whitening described above can be taken as evidence of an energy absorbing process, then this contribution to total fracture energy decreases with increasing ligament length and drives the slope to a more negative value than what is seen for the materials in Fig. 6 or the materials containing 0 and 5 wt% EPR-*g*-MA of this plot.

The transition in stress whitening at short ligament lengths for the material containing 15 wt% glass fibers

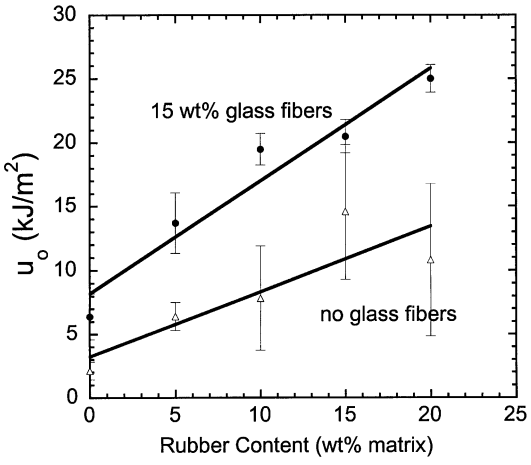


Fig. 12. Limiting specific fracture energy ($u_o$) versus rubber content for nylon 6 materials containing 0 and 15 wt% glass fibers. EPR-*g*-MA content is based on the mass of polymer matrix only (nylon 6 + EPR-*g*-MA), and glass fiber content is based on total mass of polymer and glass.

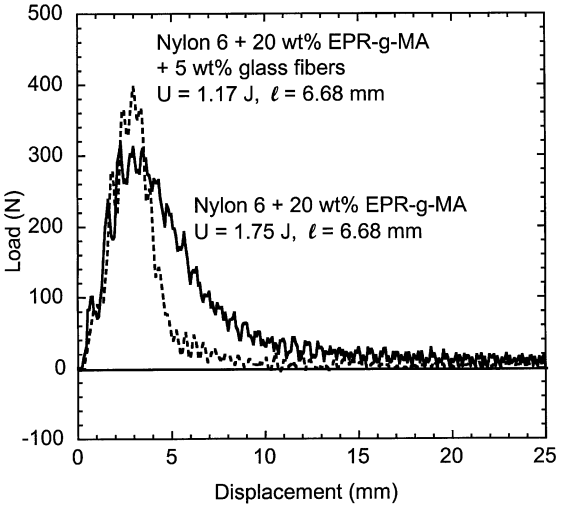


Fig. 14. Load–displacement diagram for SEN3PB specimens of (nylon 6/EPR-*g*-MA)/glass fiber [(80/20)/5] and nylon 6/EPR-*g*-MA (80/20). EPR-*g*-MA content is based on the mass of polymer matrix only (nylon 6 + EPR-*g*-MA), and glass fiber content is based on total mass of polymer and glass.

and 10 wt% rubber occurs at roughly the same ligament length as for the material containing 10 wt% EPR-*g*-MA and no glass fibers in Fig. 4. The specimens with short ligament lengths in Fig. 11, which exhibit high levels of stress whitening were not considered in the regression of this line. Similar transitions in fracture modes have been seen elsewhere and have led to a negative slope in plots of specific fracture work versus ligament length [34]. For materials containing 15 or 20 wt% EPR-*g*-MA, there is stress whitening everywhere on the fracture surface regardless of ligament length and $u_d$ is positive. This transition in stress whitening for the glass fiber reinforced blends in Fig. 11 occurs at the same as the rubber content as the materials in Fig. 4 and as reported earlier [12].

In terms of the model represented by Eq. (5), a plot of $u_o$ versus rubber content for materials containing 0 and 15 wt% glass fibers is shown in Fig. 12. There is a steady increase in $u_o$ as the rubber content is increased for both glass fiber reinforced materials and unreinforced materials. According to the physical interpretation implied in this model, the energy absorbed per unit area in the region surrounding the fracture surface increases as rubber content is increased and as glass fiber reinforcement is added. Fig. 13 shows the effect of rubber content on $u_d$. As noted above, there is a dramatic increase in this parameter for the unreinforced materials containing 15 wt% or more of EPR-*g*-MA; however, the materials containing 15 wt% glass fibers do not show this trend; the values of $u_d$ are slightly above or below zero. Thus, glass fiber reinforcement retards energy dissipation in the outer plastic zone. This decrease in $u_d$ may be associated with a decrease in ductile deformation processes away from the fracture surface.

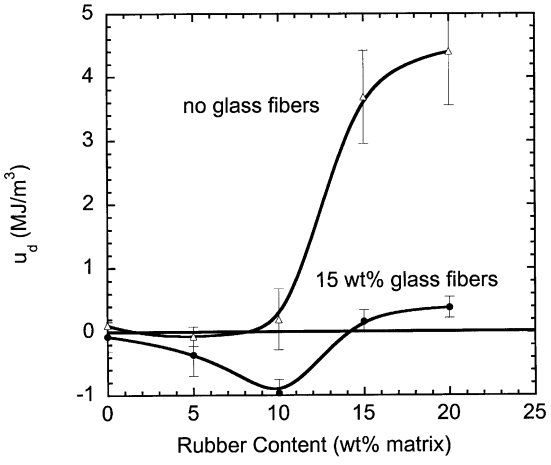


Fig. 13. Dissipative energy density ($u_d$) versus rubber content for nylon 6 materials containing 0 and 15 wt% glass fibers. EPR-*g*-MA content is based on the mass of polymer matrix only (nylon 6 + EPR-*g*-MA), and glass fiber content is based on total mass of polymer and glass.

### *4.4. Effect of adding glass fibers to rubber-toughened blends*

Fig. 14 shows load–displacement diagrams for specimens containing 20 wt% EPR-*g*-MA. The material containing 5 wt% glass fibers shows an increase in load at the yield point and fracture occurs at a much lower tup displacement relative to the unreinforced material. The reinforced material has a fracture energy of 1.17 J, which is much less than the fracture energy for the material containing no glass fibers (1.75 J). Fig. 15 shows the effect of adding more glass fibers to this rubber toughened material. The material containing 20 wt% glass fibers reaches a higher load than the material containing 5 wt% glass fibers; however, it fails at a slightly lower tup displacement. The net result is that the specimen containing 20 wt% glass fibers has a fracture energy of 1.22 J, nearly the same as the material containing 5 wt% glass fibers.

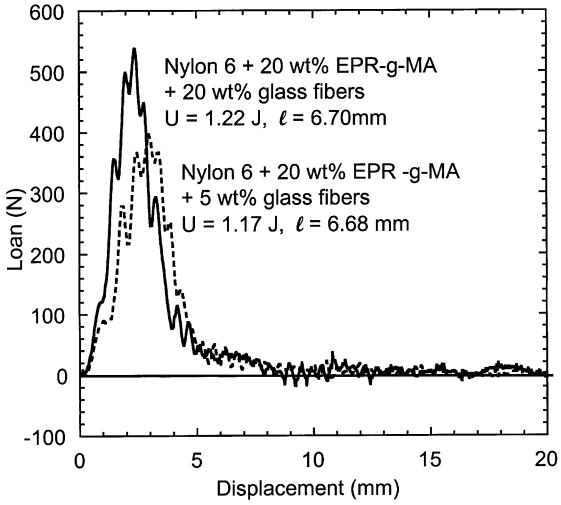


Fig. 15. Load–displacement diagram for SEN3PB specimens of (nylon 6/EPR-*g*-MA)/glass fiber [(80/20)/20] and (nylon 6/EPR-*g*-MA)/glass fiber [(80/20)/5]. EPR-*g*-MA content is based on the mass of polymer matrix only (nylon 6 + EPR-*g*-MA), and glass fiber content is based on total mass of polymer and glass.

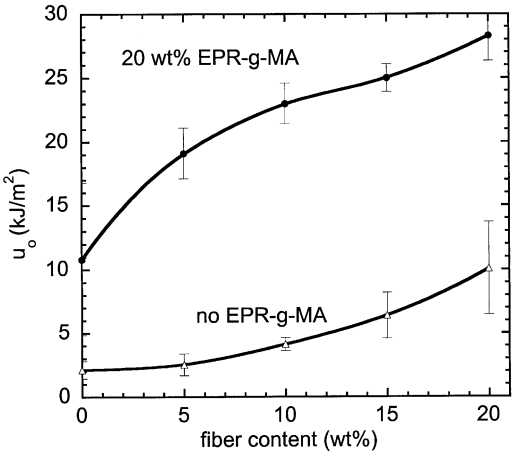


Fig. 17. Limiting specific fracture energy ($u_o$) versus glass fiber content for nylon 6 materials containing 0 and 20 wt% EPR-*g*-MA. EPR-*g*-MA content is based on the mass of polymer matrix only (nylon 6 + EPR-*g*-MA), and glass fiber content is based on total mass of polymer and glass.

Plots of total fracture energy per unit area versus ligament length for the materials containing 20 wt% EPR-*g*-MA and 0, 5 and 20 wt% glass fibers are shown in Fig. 16. The material containing no rubber is notably different from the other two in that it has a much higher slope. According to the fracture model presented above, this indicates that more energy is dissipated away from the fracture surface. The addition of 5 wt% glass fibers eliminates most of this contribution, and by 20 wt% glass fibers the slope is essentially zero. The intercepts of these plots, $u_o$, on the other hand, increase with increasing glass fiber content indicating an increase in energy absorbed at the fracture surface.

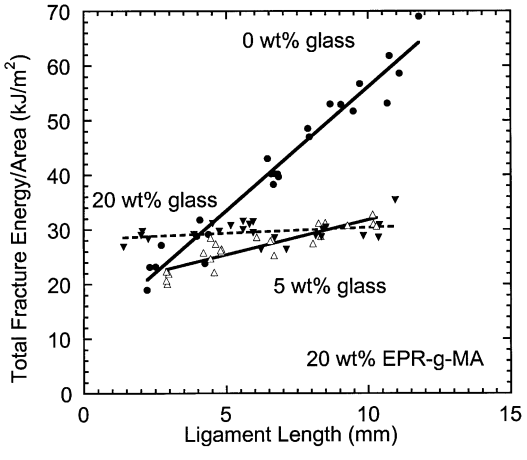


Fig. 16. Total fracture energy per unit area of fracture surface (area = $\mathcal{L}^* t$) versus ligament length for nylon 6 containing 20 wt% EPR-*g*-MA and 0, 5, and 20 wt% glass fibers. EPR-*g*-MA content is based on the mass of polymer matrix only (nylon 6 + EPR-*g*-MA), and glass fiber content is based on total mass of polymer and glass.

Although the energy absorbed near the fracture surface is increased by the presence of glass fibers, it is not enough to offset the huge drop in energy absorbed in the outer plastic zone. This indicates that the presence of even a small amount of glass fibers is sufficient to inhibit ductile energy dissipation away from the fracture surface. The material containing 20 wt% glass fibers has a higher value of $u_o$ and hence higher fracture energies for short ligaments, but $u_d$ is essentially zero. The material containing 5 wt% glass fibers, on the other hand has a higher value of $u_d$ such that the fracture energies of these two materials is very nearly the same for longer ligaments. The material containing no glass fibers has a far superior fracture energy at longer ligaments; however, as ligament length is decreased the gap between the unreinforced material and the glass fiber reinforced materials narrows. For very short ligament lengths, the material with 20 wt% glass fibers and 20 wt% EPR-*g*-MA has the highest fracture energy of any seen in this study.

Fig. 17 shows the effect of glass fiber content on $u_o$ for materials containing 20 wt% EPR-*g*-MA and for materials with no rubber. As discussed above, the addition of glass fibers to nylon 6 materials containing no rubber causes some increase in $u_o$; however, adding glass fibers to rubber toughened materials causes an even larger increase in $u_o$. Thus, composites containing 20 wt% EPR-*g*-MA have significantly higher values of $u_o$. This is consistent with the results shown in Fig. 12. Fig. 18 shows the effect of glass fiber content on $u_d$. For the materials containing no rubber, $u_d$ is essentially zero. The material containing 20 wt% EPR-*g*-MA and no glass fibers has a high value of $u_d$ relative to any other material shown. The addition of 5 wt% glass fibers substantially reduces this value, and as more glass fibers are added, $u_d$ decreases further, but at a much slower rate.

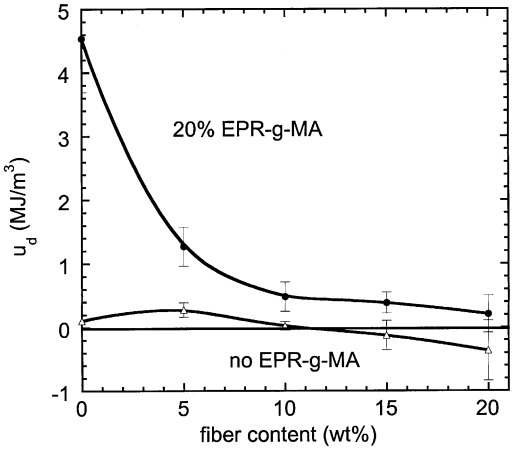


Fig. 18. Dissipative energy density ($u_d$) versus glass fiber content for nylon 6 materials containing 0 and 20 wt% EPR-*g*-MA. EPR-*g*-MA content is based on the mass of polymer matrix only (nylon 6 + EPR-*g*-MA), and glass fiber content is based on total mass of polymer and glass.

## 5. Conclusions

The effects of glass fiber reinforcement and rubber toughening on the impact fracture mechanics of nylon 6 were examined. Rubber toughening alone leads to a higher peak load and increases the amount of deformation that the material undergoes during impact tests. Analysis of these data according to the model represented in Eq. (5) indicates that the incorporation of EPR-*g*-MA increases $u_o$ and $u_d$. A dramatic increase in $u_d$ beyond 15 wt% EPR-*g*-MA is seen which coincides with a ductile-to-brittle transition.

Glass fiber reinforcement alone increases the peak load of nylon 6 without significantly decreasing specimen deformation relative to neat nylon 6, which is brittle under the impact conditions used here. This leads to higher fracture energies for the fiber reinforced materials. The analysis of this fracture data according to Eq. (5) indicates an increase in the apparent value of $u_o$ with increasing fiber content while $u_d$ remains essentially zero; however, these data have an initial negative slope followed by an increase in fracture energy at longer ligament lengths. The EWF model is unable to explain this behavior. The LEFM model, on the other hand, accurately captures these trends. The LEFM model analysis shows an increase in the critical strain energy release rate with increasing glass fiber content.

When both glass fiber reinforcement and rubber toughening are used in the same material, it was found that the addition of only 5 wt% glass fibers reduces most of the contribution from energy dissipated in the outer plastic zone, as indicated by a decrease in $u_d$. This loss is offset somewhat by an increase in $u_o$. The net result of these two effects is that at long ligaments, the material containing 20 wt% EPR-*g*-MA and no fiber reinforcement has a much higher fracture energy. At very short ligament lengths; however, the material containing 20 wt% EPR-*g*-MA and 20 wt% glass fibers has the highest fracture energy. Thus, sample geometry plays a very important role in the trends observed and material selection must carefully consider the part design criteria.

When glass fibers and rubber toughening are added in a single extrusion step, interfacial chemistry and rubber compatibilization chemistry may interact. In this paper, however, the glass fibers were adhered to the matrix prior to the addition of rubber precluding any variation in interfacial chemistry. Future work will investigate the effects of interfacial chemistry and fiber/matrix adhesion.

## Acknowledgements

This material is based in part upon work supported by the Texas Advanced Technology program under Grant No. 003658-017. Allied Signal, Bayer, and Exxon donated materials for this research.

## References

[1] Paul DR, Newman S, editors. Polymer blends. New York: Academic Press, 1978.
[2] Collyer AA, editor. Rubber toughened engineering plastics. London: Chapman and Hall, 1994.
[3] Krenchel H. Fiber reinforcement. Copenhagen: Akademisk Forlag, 1964.
[4] Folkes MJ. Short fiber reinforced plastics. In: Miles IS, Rostami S, editors. Multicomponent polymer systems. Essex: Longman, 1992 (Chapter 8).
[5] Nair SV, Wong S-C, Goettler LA. J Mater Sci 1997;32(20):5335–46.
[6] Gaymans RJ. Toughened polyamides. In: Collyer AA, editor. Rubber toughened engineering plastics. London: Chapman and Hall, 1994 (Chapter 7).
[7] Nair SV, Subramaniam A, Goettler LA. J Mater Sci 1997;32(20):5347–54.
[8] Nair SV, Shiao ML, Garret PD. J Mater Sci 1992;27(4):1085–100.
[9] Gaymans, RJ, Oostenbrink, AJ, van Bennekom ACM, Klaren, JE. Fibre reinforced nylon–rubber blends. In: PRI Conference on Deformation and Fracture of Composites, Manchester, 1991;2321–25.
[10] Bailey RS, Bader G. The effect of toughening on the fracture behavior of a glass–fiber reinforced polyamide. In: Harrigan WC, Strife J, Dhingra AK, editors. Fifth International Conference on Composite Materials. San Diego: Metallurgical Society Inc, 1985. p. 947–61.
[11] Karger-Kocsis J. In: Paul DR, Bucknall CB, editors. Reinforced polymer blends, Polymer blends: formulation and performance, vol. 2. New York: Wiley, 1999 (Chapter 31).
[12] Laura DM, Keskkula H, Barlow JW, Paul DR. Polymer 2000; 41(19):7165–74.
[13] Plati E, Williams JG. Polym Engng Sci 1975;15(6):470–7.
[14] Mai YW, Cotterell B. Int J Fract 1986;32(2):105–25.
[15] Mai YW. Engng Fract Mech 1985;21(1):123–8.
[16] Mai Y-W, Wong S-C, Chen X-H. Application of fracture mechanics for characterisation of toughness of polymer blends. In: Paul DR, Bucknall CB, editors. Polymer blends: formulations and performance, Vol. 2. New York: Wiley, 1999 (Chapter 20).
[17] Broberg KB. J Mech Phys Sol 1975;23(3):215–37.
[18] Broberg KB. J Mech Phys Sol 1971;19(6):407–18.
[19] Oshinski AJ, Keskkula H, Paul DR. J Appl Polym Sci 1996;61(4):623–40.
[20] Oshinski AJ, Keskkula H, Paul DR. Polymer 1992;33(2):268–83.
[21] Oshinski AJ, Keskkula H, Paul DR. Polymer 1996;37(22):4909–17.
[22] Oshinski AJ, Keskkula H, Paul DR. Polymer 1996;37(22):4919–28.

[23] Okada, O., Keskkula, H., Paul, D.R. Polymer 2000;41(22):8061–74.
[24] Kudva RA, Keskkula H, Paul DR. Polymer 2000;41(1):335–49.
[25] Pressly TG, Keskkula H, Paul DR. 2001;42(7):3043–55.
[26] Wells JK, Beaumont PWR. J Mater Sci 1985;20(8):2735–49.
[27] Kelly A, Tyson WR. J Mech Phys Sol 1965;13(6):329–50.
[28] Gupta VB, Mittal RK, Goel M. Comp Sci Technol 1990;37(4):353–69.
[29] Fu F-Y, Lauke B. J Mater Sci 1997;32(8):1985–93.
[30] Wetherhold RC, Jain LK. Mat Sci Engng 1992;A151(2):169–77.
[31] Lauke B, Schultrich B. Comp Sci Technol 1985;23(1):21–35.
[32] Shiao M-L, Nair SV, Garrett PD, Pollard PE. Polymer 1994;35(2):306–14.
[33] Chua PS, Dai SR, Piggott MR. J Mater Sci 1992;27(4):913–8.
[34] Mouzakis DE, Karger-Kocsis J. Polym Bull 1999;42(4):473–80.